We are IntechOpen,
the world's leading publisher of
Open Access books
Built by scientists, for scientists

4,800
Open access books available

122,000
International authors and editors

135M
Downloads

Our authors are among the

154
Countries delivered to

TOP 1%
most cited scientists

12.2%
Contributors from top 500 universities

BOOK CITATION INDEX
CLARIVATE ANALYTICS
INDEXED

WEB OF SCIENCE™

Selection of our books indexed in the Book Citation Index
in Web of Science™ Core Collection (BKCI)

Interested in publishing with us?
Contact book.department@intechopen.com

Numbers displayed above are based on latest data collected.
For more information visit www.intechopen.com

Evaluation and Stability Analysis of Onshore Wind Turbine Supporting Structures

Chikako Fujiyama, Yasuhiro Koda and Noriaki Sento

Additional information is available at the end of the chapter

Abstract

This chapter shows research of stability of supporting structure of onshore wind turbine foundations based on field measurements, finite element (FE) analysis and laboratory experiment. In order to investigate the relation of action-response of tower-foundation system, long-term field measurements were carried out for two existing onshore wind turbines with/without piles for its foundations. Then, the models were built up for three-dimensional nonlinear FE analyses. The damage processes of reaching failure were examined by FE models, and limit state of foundations was individually defined by fatigue limit state of concrete. Consequently, the stress-number of cycle (S-N) diagram derived from both experiment and analysis was discussed for the assessment of existing structure.

Keywords: concrete, foundation, fatigue, anchor bolt, crack

1. Introduction

Wind power is growing a major industry. At the year of 2006, the total amount of installed wind power capacity reached 74.1 GW in the world [1], while it has reached 486.8 GW in the world at the year of 2016 [2] due to a rapid installation of wind turbine in this decade. In particular, increasing wind energy production has been even more actively touted against the background of the Great East Japan earthquake and the resultant nuclear power plant accident. However, in the past, wind turbines have had troubling experiences of structural collapse as well as failure of blade [3].

In particular, the structures supporting wind turbines, especially the foundation made of concrete, have been paid attentions in recent years. There are the reports that investigate cracks on foundation concrete [4–7]. It is not easy to identify the cause of cracks, while repeated action transferred from the tower is thought to be one of the causes. Therefore, fatigue of supporting structure made of concrete has become a main concern of researchers [7–10]. Even though the cracks are not always the trigger of structural collapse of wind turbine, further investigations are required for safe and steady operation of power plant.

Here, it is important, for practical design, to precisely analyze the responses of structures and to capture the action of wind. The response of existing wind turbine tower was analyzed using wireless system of accelerometers [11]. The development of a health monitoring system for the wind turbine tower-foundation system has been reported [12]. In addition, three-dimensional nonlinear finite element (FE) analyses for wind turbine tower-foundation systems have been conducted using idealized static forces as input [13].

This chapter shows research of stability of supporting structure of onshore wind turbine foundations based on field measurements, laboratory experiment and FE analysis. In order to investigate the relation of action-response of tower-foundation system, long-term field measurements were carried out for an existing onshore wind turbine without piles for its foundations. Then, the model was built up for three-dimensional nonlinear FE analyses. The damage process of reaching failure was examined by FE models. In addition, limit state of foundation was defined by fatigue limit state of concrete. Consequently, the stress-number of cycle (S-N) diagram derived from laboratory experiment and analysis was discussed for the assessment of existing structure.

2. Field measurement

2.1. Overview of target and measurement setup

The responses of structure were investigated using field data, which were measured at a wind turbine equipped in 2003 on the campus of Nihon University and along the Abukuma River in the Fukushima prefecture, Japan. The wind turbine specifications and the positions of the measuring equipment are shown in **Figure 1**. The rated power is 40 kW and rated wind speed is 11 m/s. The cut-in wind speed and cut-out wind speed are 2 and 25 m/s, respectively. This had been continuously operated even during the Great East Japan Earthquake in 2011, which resulted in no visible damage.

The accelerometers were attached at the top and middle of the tower horizontally. There are 60,000 data points for 5 min at a sampling frequency of 200 Hz. The data were recorded every hour when exceeding the acceleration threshold of ±0.7 m/s^2. To investigate the transmission of vibration from the tower to the foundation, strain gauges were attached at the anchor bolts in the east, west, north, and south direction. The sampling conditions were the same as those in the accelerometer. Wind speed and direction were measured using an anemometer attached to the nacelle with a sampling frequency of 1.0 Hz. The measurements have been begun since May 2013.
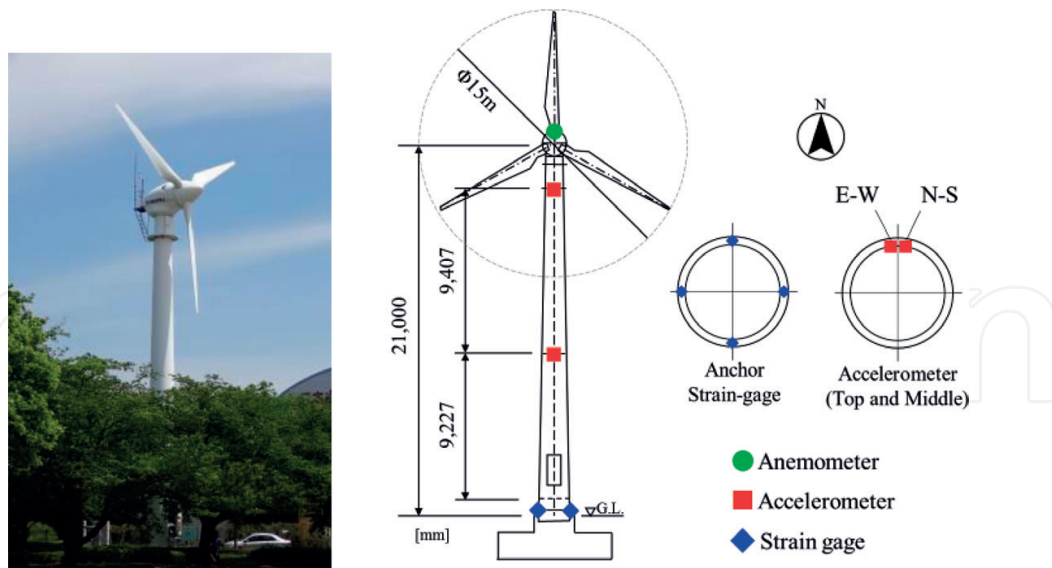
Figure 1. Overview and schematic of the apparatus used in measurements (based on [13]).

2.2. Responses of the tower

Figure 2 shows the maximum wind speed versus the maximum response of acceleration. Despite the scatter of the data, shown as black dots for operating wind speeds of 2–20 m/s, the maximum acceleration increased linearly with wind speed. The red dots represent data recorded while the generator was not operating. The difference between the two datasets suggests that the blade pitch control system dampened the acceleration response.
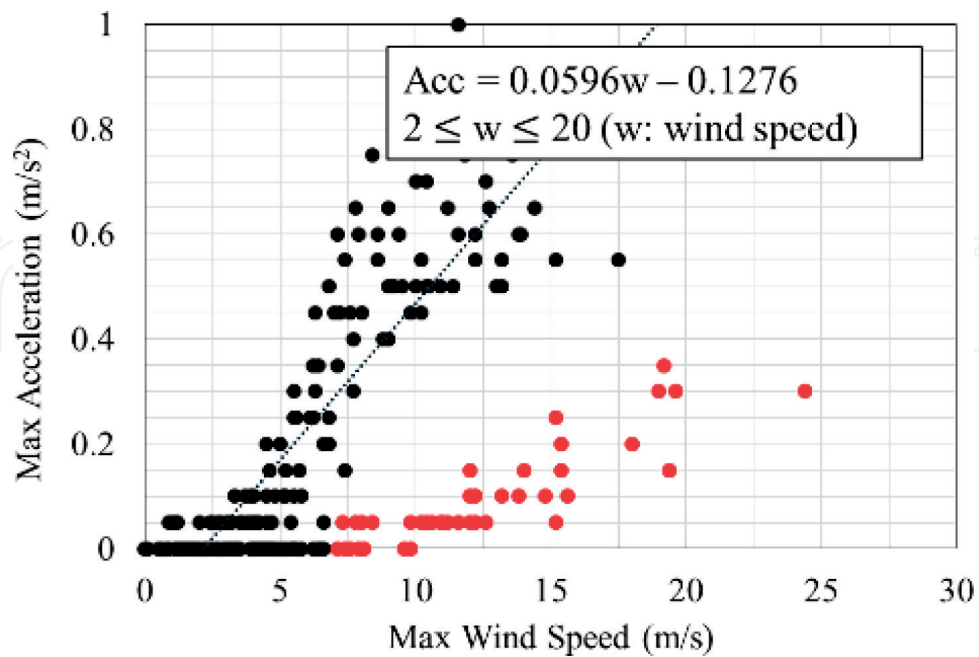

Figure 2. Max acceleration versus max wind speed in October 2013 [13].

The acceleration response of the tower in the time domain and trajectory of the tower displacement, which are derived through double integration of acceleration in the time domain are shown in **Figure 3**. To remove noise, a digital band pass filter with pass band between about 0.1 and 30 Hz was designed. The maximum displacement was about 0.5 cm at the top of the tower in the EW direction. Elliptical trajectories with different main axis were observed for each height in different scales when the wind turbine was operating. In particular, the trajectories of the top and middle of the tower were almost similar. This means that the predominant vibration mode was the primary mode.

2.3. Action to the foundation transmitted from the tower

The strain of nut for anchor bolt clearly depended on the acceleration variations, even though the value of the response was less than 1 μ. This can be explained that the location of strain gauges attached to anchor bolts was not consistent with wind direction which measured max wind speed.

When taking a long-term measurement, time varying character of the wind can be captured in a spectrum. The Fourier spectrum exhibited the waveform shown in **Figure 4**. The natural
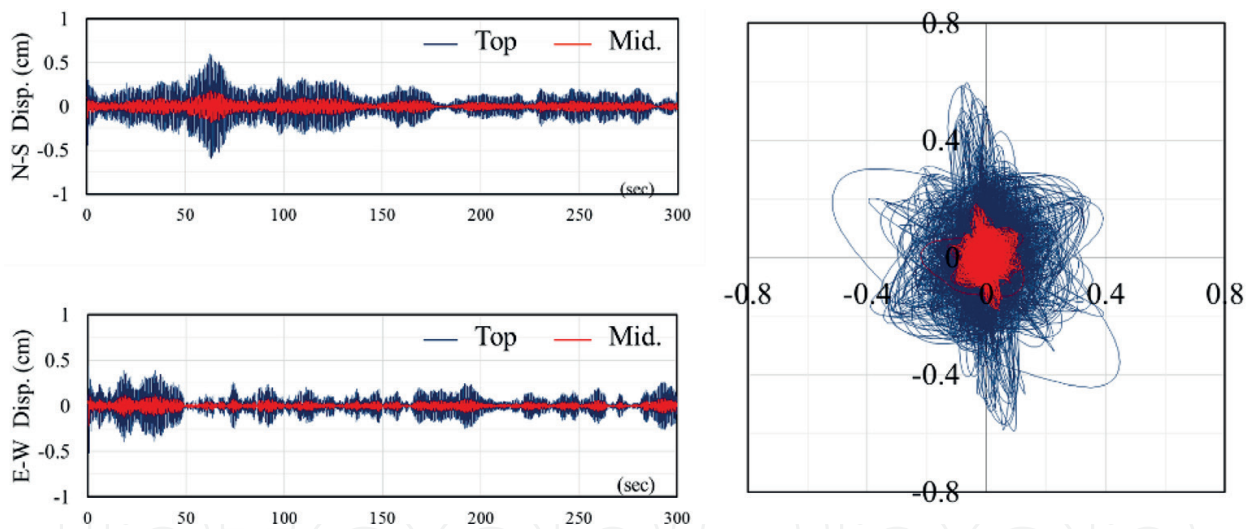

Figure 3. Acceleration response of tower and trajectory of its displacement (based on [13]).
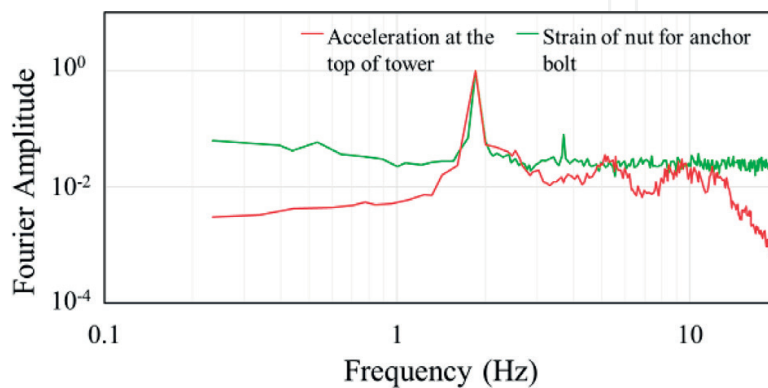

Figure 4. Fourier spectrum of acceleration of tower and strain on anchor bolt (based on [13]).

frequency was 1.8 Hz in the primary mode and 13 Hz in the secondary mode based on the eigenvalue analysis and free vibration tests. The figure suggested the predominant vibration mode transmitted from the tower to the foundation was the primary mode.

3. Finite element analysis

3.1. Modeling

The nonlinear finite element (FE) analysis code COM3D developed by Maekawa et al. [14, 15] are used in this study. The decrease of stiffness and the accumulation of plasticity of concrete subjected cyclic load are carefully formulated for concrete in the code. In particular, employing the logarithmic integral scheme that enabled to calculate fatigue damage of concrete is one of the advantages of this code. The properties for steel are expressed with bi-linear form.

An overview of the FE model is shown in **Figure 5**. The model was modified from the model in the previous study [13] through further material investigation and verifications. Mechanical properties of these constituent materials are summarized in **Table 1**.

In order to simplify structural model, the shape of nacelle and blades was not directly modeled. Alternatively, dead weight of them was applied to certain elements located at the top of with each material density. All the members except anchor bolts and the intermediate restraining reinforcements of the pedestal were modeled by solid element. Exceptions were expressed by line element; in particular, the torque on an anchor bolt was replaced by initial strain of the lines. The boundary condition between steel and concrete was modeled by joint element based on the Mohr–Coulomb theory with 0.6 as friction coefficient. Vertical displacement was restricted at the nodes of the footing bottom surface; however, confinement of surrounding soil was not considered on the side of the footing as same in literature [16].
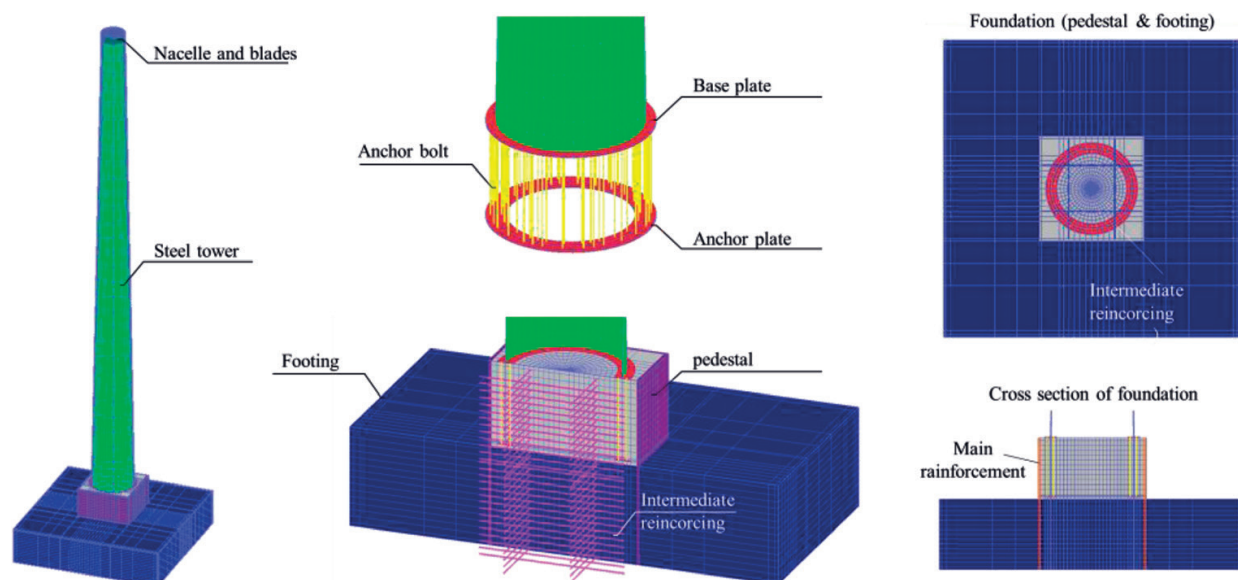

Figure 5. Overview of FE model (based on [10]).

	Young's modulus (GPa)	Compressive strength (MPa)	Yield strength (MPa)	Tensile strength (MPa)	Poisson ratio
Concrete	23.5	21.0	—	8.13	0.2
Anchor bolt	205	—	235	400	0.3
Other steels	205	—	325	490	0.3
Reinforcing bar	205	—	345	517.5	0.3

Table 1. Mechanical properties of each material in FE analysis.

3.2. Verification of the model

The model was verified by the comparison of the analytical result and data obtained during free vibration test. The natural frequency of tower and damping factor calculated by FE analysis were 1.84 Hz and 0.30%. Those obtained from the field test were 1.78 Hz and 0.27% [10].

In addition, the agreement of analytical results and data obtained in field measurement were examined. First, the displacement at the top of tower which was converted using double integration of acceleration in the time domain as mentioned in 2.1.2, was inputted to the model. Then, acceleration of tower, strain of tower body, and strain of anchor bolts calculated by FE analysis were compared with data obtained in the field for six different cases including data during typhoon and earthquakes. Samples of examinations in terms of maximum and minimum values are shown in **Figure 6**. The analysis results tended to show spikes due to the difficulty of convergence of calculation. However, acceptable agreement was seen in all six cases.

3.3. Prediction of failure mode

In order to determine the failure mode of this structure, monotonic horizontal displacement was applied to a node at the top of tower. The bending moment at the bottom of tower versus rotation angle derived from Eq. (1) [10] is shown in **Figure 7**.

$$\phi = arctan\left(\frac{\delta_{zt} - \delta_{zc}}{B}\right) \tag{1}$$
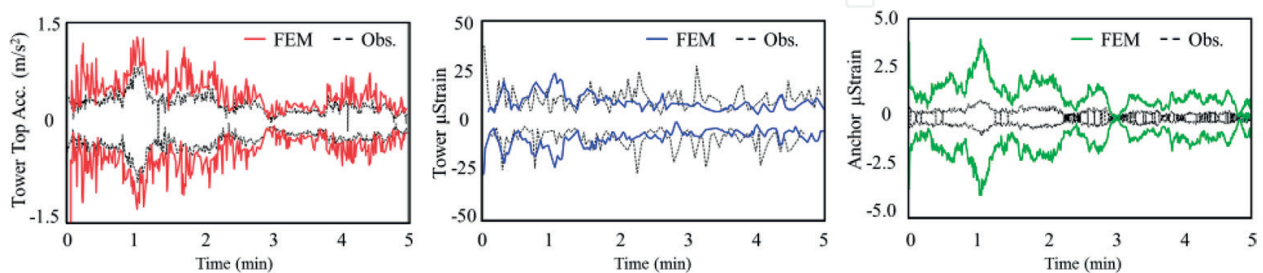

Figure 6. Comparison of FE model and observed data during power generating (left: acceleration at the top of tower; middle: strain of tower body; right: strain of anchor bolt) (based on [10]).
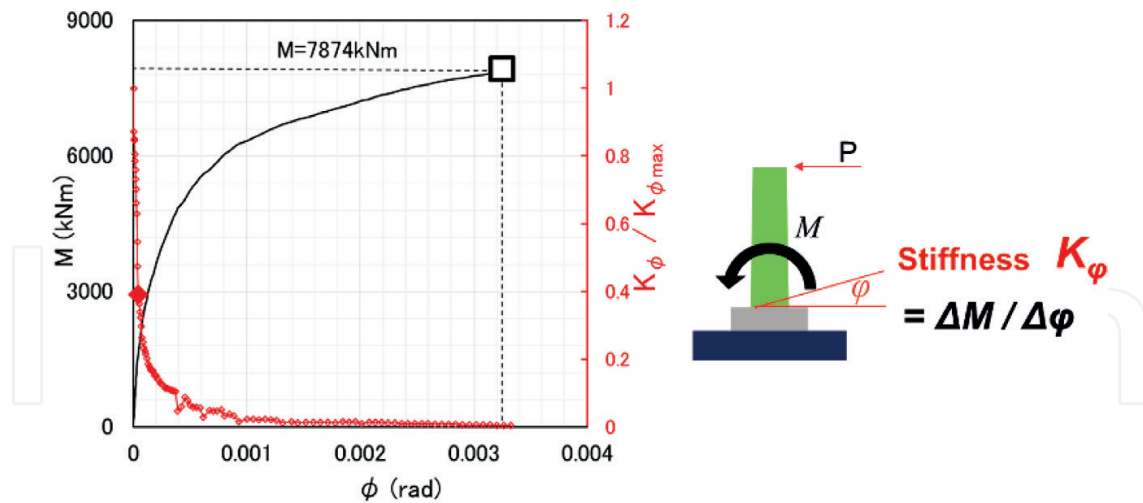
Figure 7. Bending moment at the bottom of tower and rotation angle.

where φ is rotation angle, δzt is vertical displacement of anchor plate in tension side, δzc is vertical displacement of anchor plate in compression side, and B is a diameter of anchor ring.

The moment increased rapidly at the beginning of loading, and it gradually became mild. Then, the moment remained static after when 50% of anchor bolts reached their yielding strength. At the time, the horizontal displacement at the top of tower was 50 cm where the moment and rotation angle reached 7874 kNm and 0.0033 rad. **Figure 7** also shows the normalized stiffness by using the right axis. The stiffness mentioned here means the value that was obtained when moment was divided by the rotation angle. The normalized stiffness means the stiffness normalized by the initial stiffness. According to **Figure 7**, the normalized stiffness significantly dropped in the first 0.0001 rad.

What did cause the significant drop to normalized stiffness? It was the cracking of concrete at the tip of anchor ring inside pedestal (see **Figure 8**). Consequently, the crack developed horizontally and came to the center of the pedestal in the end of analysis (see **Figure 9**). Regarding this FE analysis, the failure mode was a coupling mode of yielding 50% of anchor bolts and development of horizontal crack to more than half of the pedestal's width.
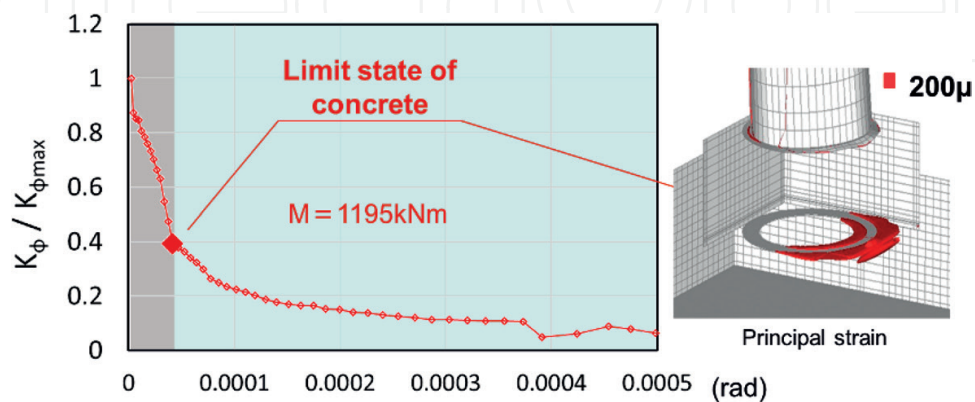

Figure 8. Principal strain distribution at the drop of normalized stiffness.
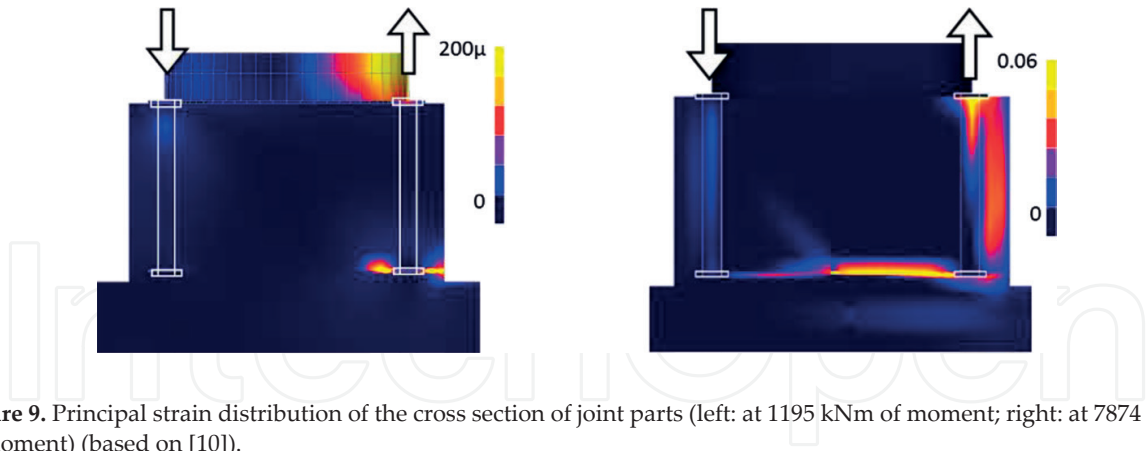
Figure 9. Principal strain distribution of the cross section of joint parts (left: at 1195 kNm of moment; right: at 7874 kNm of moment) (based on [10]).

The ultimate bending moment calculated by the FE analysis was 7874 kNm, it is much higher than the design moment in the case of earthquake in this area; 2430 kNm. This means that the targeted wind turbine has sufficient allowance of safety. However, the cracking moment 1195 kNm is close to the design moment owing to the wind in this area; 855 kNm. Therefore, evaluation of fatigue resistance of concrete foundation is needed.

3.4. Identification of index

Since the cracking inside pedestal was observed as the cause of the decrease of stiffness, evaluation of fatigue resistance of this structure focused on this event. The specific index, space averaged second invariant strain [17] was employed to determine the possibility of cracking. This index is independent of direction of stress or strain that is unsettled at each moment under the vibration of tower, but is a scalar obtained by Eqs. (2) and (3) [17].

$$\sqrt{J_2'} = \sqrt{\frac{2}{3}\left\{\left(\frac{\varepsilon_x - \varepsilon_y}{2}\right)^2 + \left(\frac{\varepsilon_y - \varepsilon_z}{2}\right)^2 + \left(\frac{\varepsilon_z - \varepsilon_x}{2}\right)^2\right\} + \left(\frac{\gamma_{xy}}{2}\right)^2 + \left(\frac{\gamma_{yz}}{2}\right)^2 + \left(\frac{\gamma_{zx}}{2}\right)^2} \tag{2}$$

$$\overline{\sqrt{J_2'}} = \frac{\int_V \sqrt{J_2'} \cdot w(x)dV}{\int_V w(x)dV} \quad w(x) = \begin{cases} 1 - x/L & x \leq L \\ 0 & x > L \end{cases} \tag{3}$$

where, $\sqrt{J_2'}$ is the second invariant of strain, $\overline{\sqrt{J_2'}}$ is the space-averaged second invariant of strain, ε and γ are normal and shear strains respectively, $w(x)$ is a weighting function, x is a distance from the tip of anchor plate in tension side (mm), L is a radius of average volume (mm). For this analysis, L was determined as 200 mm based on [18].

The horizontal displacement of tower versus the space-averaged second invariant of strain is shown in **Figure 10**. The space-averaged second invariant of strain at the occurrence of the horizontal crack determined by **Figure 9** was identified as 0.000032. Thus, threshold value for first limit state of this structure was defined as 0.000032 by the space-averaged second invariant of strain.
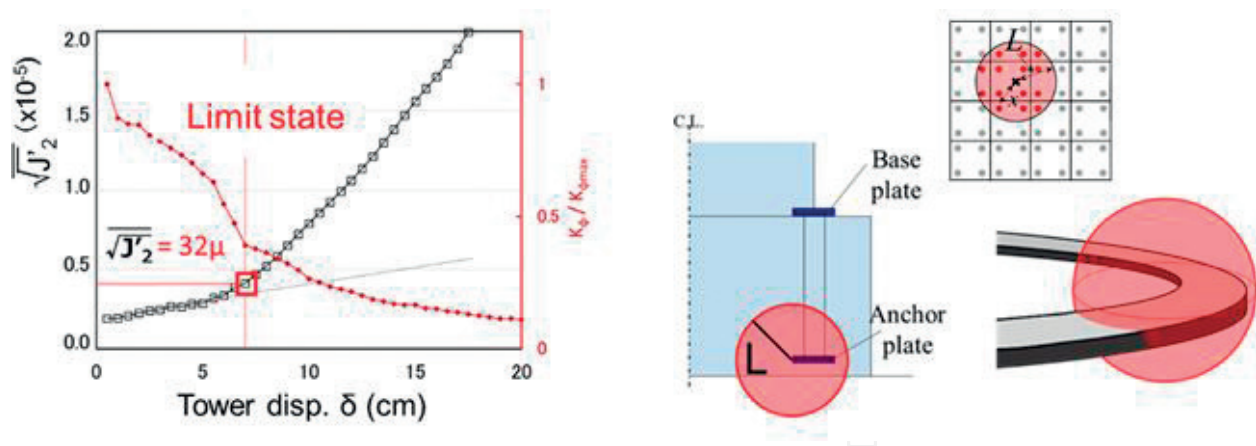
Figure 10. Horizontal displacement of tower versus the space-averaged second invariant of strain.
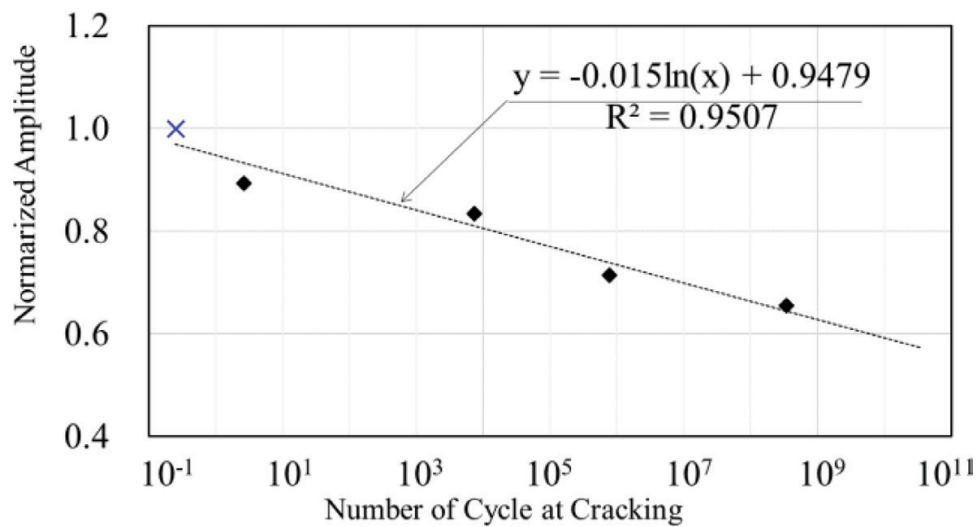

Figure 11. Normalized amplitude of horizontal load—cycles at cracking inside concrete based on FE analysis.

3.5. Evaluation of fatigue resistance of concrete foundation

The fatigue resistance of concrete foundation was examined by FE analysis. Since the horizontal reaction force at the top of tower when the moment was 1195 kNm was about 84kN in FE analysis, input horizontal load at the top of tower was offered as sine wave with different amplitudes. In addition, the number of cycles when the space-averaged second invariant of strain reach threshold value 0.00032 were calculated for each cases. The relationship between the normalized amplitude by 84kN and the number of cycle at threshold value was shown in **Figure 11**.

It should be noted that the design moment owing to the wind in this is 855 kNm that is 71% of the calculated moment 1195 kNm. Thus, according to **Figure 11**, the cracking inside pedestal concrete possibly starts after 763,888 swings of tower due to strong wind. However, the design moment considers safety factor as 3.0.

4. Laboratory experiment

4.1. Equipment, specimen and conditions

Since it is impossible to verify the failure mode and fatigue life of the target structure, laboratory experiment using the 1/12 scale model was prepared. In order to generate high cycle load with reliable stability, a bi-axial shaking table driven by magnetic force was employed for this study (see **Figure 12**). Tri-axial cyclic loading machine controlled hydraulic jack is not suitable for high cycle loading, even though the load generated by hydraulic jack can be higher than inertial force generated by a shaking table.

The overview of specimen is shown in **Figure 13**. This is basically designed as a 1/12 scale model of target structure shown in **Figure 1**. However, the reinforcement ratio in both pedestal and footing is higher than the real structure because it is impossible to simply scale down the diameter of reinforcing bars. The weight of blades and nacelle was 52.5 kgf that reflects the weight of steels set on the top of tower. The tower was made of STK400 steel pipe, and this model was reused for all foundation specimens. The tower model and foundation specimens were tight by eight M8 anchor bolts. The footing was fixed by four bolts at each corner of footing to shaking table.

Accelerometers were set at the top of tower and on top surface of footing to capture horizontal motions in two axes. Laser displacement meters and LVDTs were set for the top of tower and shaking table, respectively to compare the values with obtained from accelerometers. Strains of surfaces of pedestal concrete and surfaces of steel tower were measured by strain gauges. Furthermore, mold-type strain gauges were embedded beside eight anchor bolts to capture the trend of cracking inside concrete.

The conditions of all specimens are shown in **Table 2**. The laboratory experiment consisted of two series. The first series named "N-" was the prototype. The second series named "G-" installed gypsum between tower and foundation to smooth top surface of concrete specimens as well as monitoring strain gauges attached on the nut to control initial torque of anchor
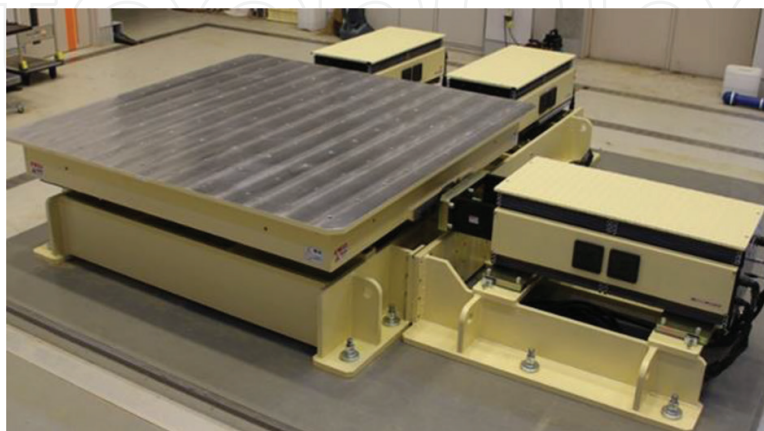

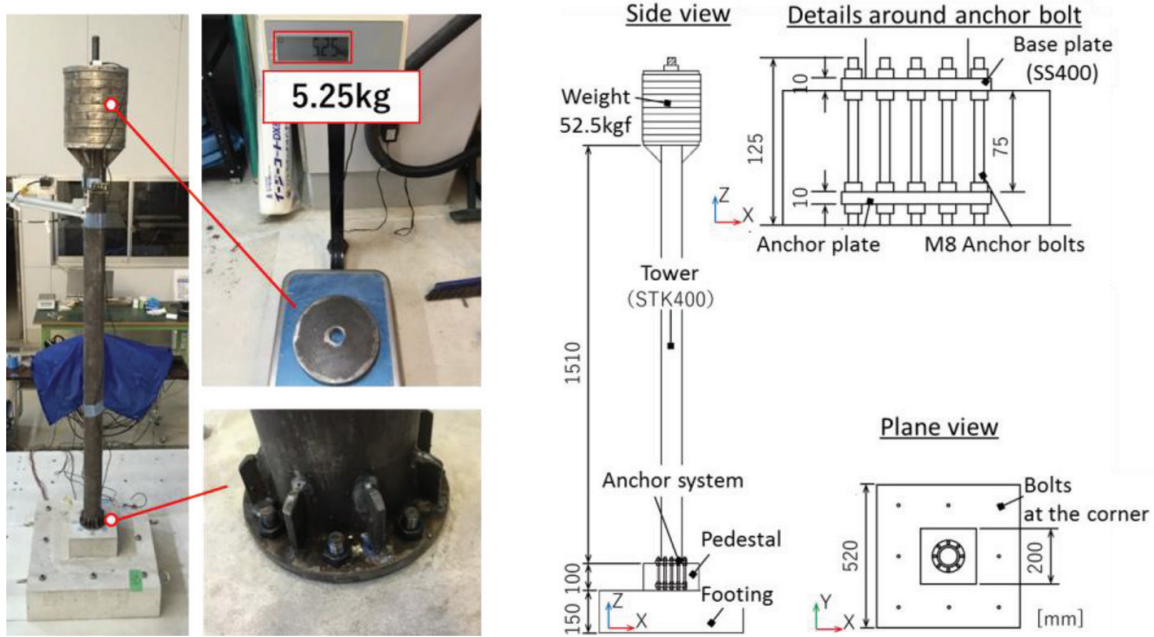**Figure 12.** Bi-axial shaking table driven by magnetic power.

Figure 13. Photos and drawings of specimen.

bolts. All the specimens except G-D-E were examined by 5 Hz sine wave vibrating with different amplitudes. Furthermore, considering the change of main axis of tower vibration in time domain (see **Figure 3**), vibrating of X and Y axis in turn was tried for three cases, that is, N-D-500, N-D-400 and G-D-900. The other hand, G-D-E is the case using X and Y axis actuator simultaneously for reproducing ground acceleration record that was obtained in this area during Great East Japan Earthquake 2011.

4.2. Results

Since it is impossible to observe cracking inside concrete during experiment, the criteria of fatigue failure of these specimens were defined as 20 mm of relative horizontal displacement at the top of tower. It is large enough because 20 mm of the model is almost equivalent to 240 mm for the real structure. Another reason is that the specimens dangerously resonate when the relative displacement exceed 20 mm [19]. Because the natural frequency of specimens which is usually 6.5–7.6 Hz before loading had gradually decreased with increase of number of load cycle due to fatigue damage of concrete.

In the case of N-S-500, sudden fracture of an anchor bolt occurred, then loading was stopped. It failed but the failure mode was different from others. The four surviving cases did not show any changes in measurable data for a long time, then loading was canceled.

The comparison of the development of relative displacement at the top of tower for G-S-900 and G-D-900 was shown in **Figure 14**. It was clear that the G-S-900 under single axis vibration survived longer than G-D-900 under the vibrating of X and Y axis in turn. Interestingly, N-S-500 also survived longer than N-D-500 (see **Figure 15**), even though the failure mode of N-S-500 was different from N-D-500.

Case	Acc. amplitude (gal)	Direction	Cycle	Fail/survive	Gypsum & torque control	Compressive stress of concrete (Mpa)
N-S-700	700	X	1000	Fail	—	27.9
N-S-500	500	X	188,900	Fail*	—	27.9
N-D-500	500	X or Y	X 70,050 Y 64,950	Fail	—	27.9
N-S-400	400	X	102,300	Survive	—	27.9
N-D-400	400	X or Y	X 51,300 Y 51,300	Survive	—	27.9
G-S-900	700–900	X	51,000	Fail	G, T	27.6
G-D-900	700–900	X or Y	X 13,500 Y 13,220	Fail	G, T	27.6
G-S-600	600	X	201,300	Survive	G	27.6
G-S-900C	900	X	79,800	Fail	G, T	27.6
G-D-EQ	Seismic wave	X and Y	5minx10	Survive	G, T	27.6

Table 2. The conditions of all specimens.

The vertical strains inside concrete measured by embedded strain gauges were shown in **Figure 16**. The vibrating direction of G-S-900 is always along X axis. Thus, the amplitude of IS1 and IS5 located in the orthogonal direction was significantly smaller than others. The strains measured in G-D-900 vibrated in both directions demonstrated relatively larger amplitude than G-S-900 in all locations. This suggested that the cracking in wider area possibly accelerated the fatigue damage and led shorter fatigue life.

In order to observe internal cracks, concrete parts were cut in two directions after the loading (see **Figure 17**). The expected cracks from the tip of anchor plate could not be seen clearly for G-S-900 and other specimens under single axis loading, except N-S-700 that failed rapidly in
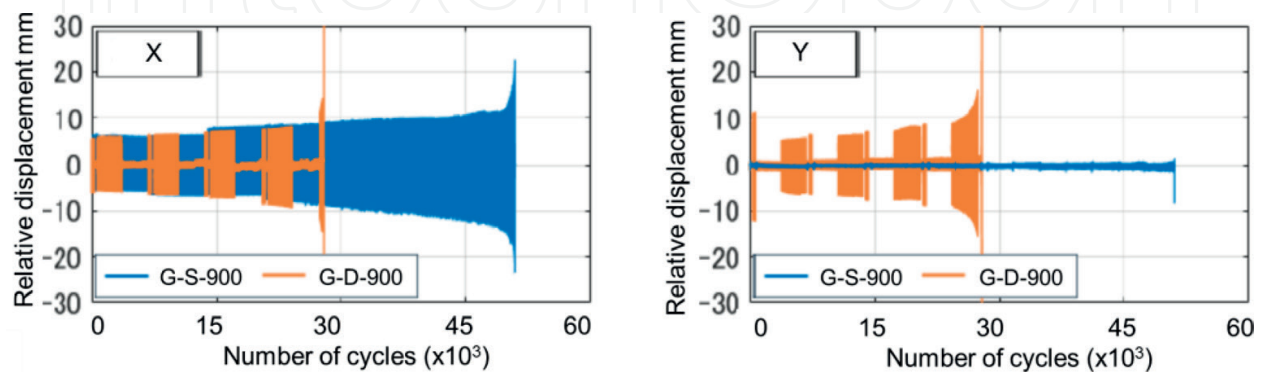

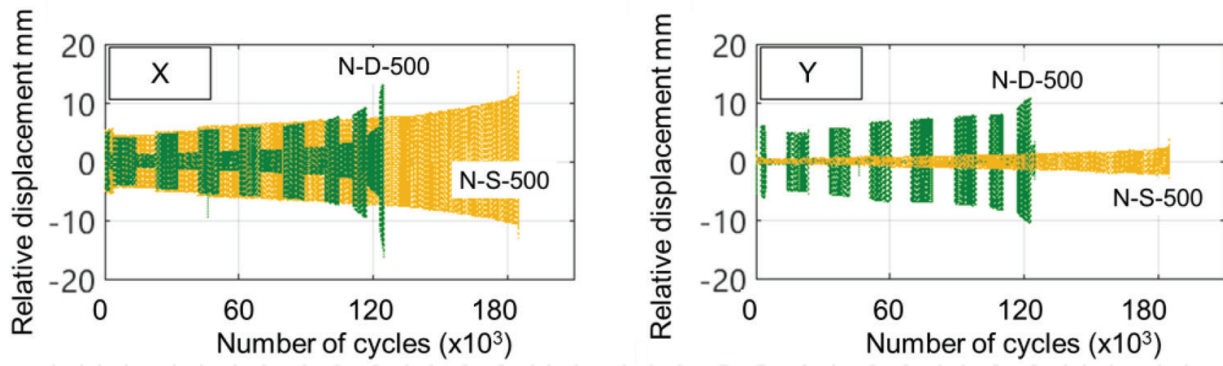**Figure 14.** The development of relative displacement at the top of tower (G-S and G-D).

Figure 15. The development of relative displacement at the top of tower (N-S and N-D).
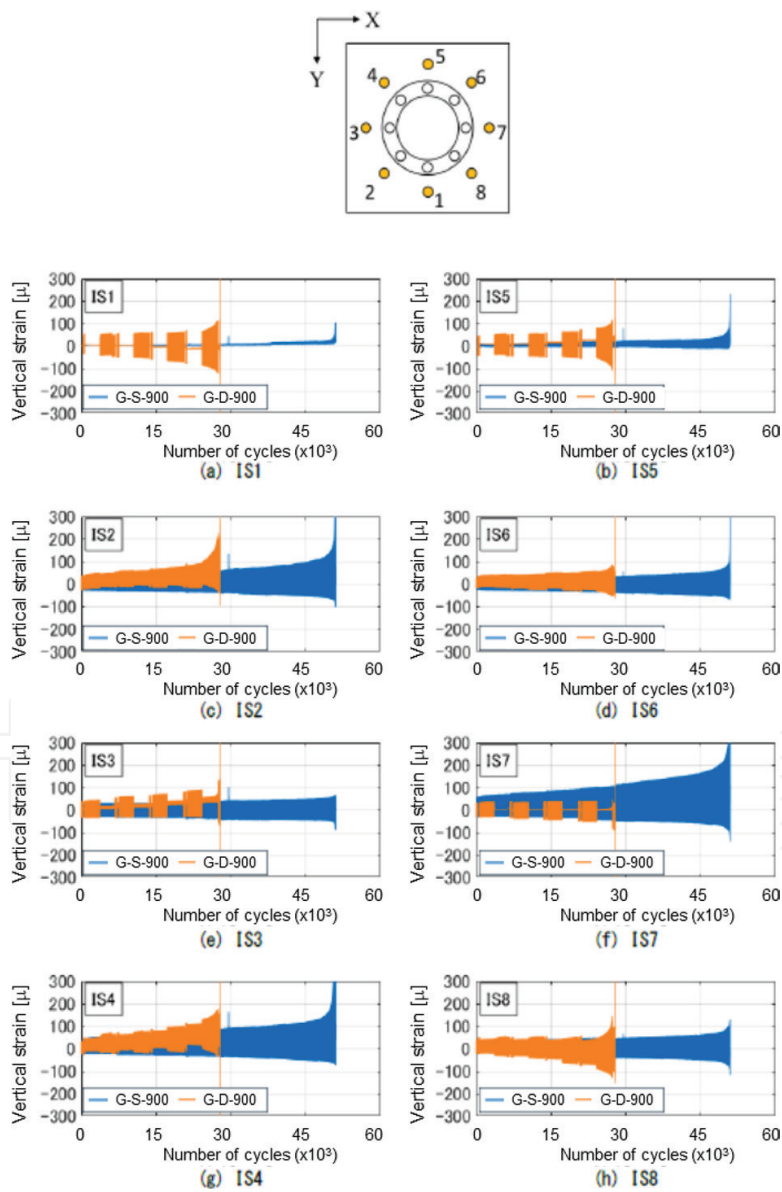

Figure 16. Vertical strain inside concrete for G-S-900 and G-D-900.

1000 cycles. Alternatively, unexpected crack at the connection of pedestal and footing was found as pointed by arrows in **Figure 17**. In contrast, obvious cracks were found in both cross sections for G-D-900. On the other hand, the difference was not clear between N-D-500 and N-S-500. These cracks did not always consistent with the internal strains measured by embedded gauge. In other words, it is not easy to capture the occurrence of cracks inside concrete. It should be noted that the strain measured at the bottom of steel tower always remained less than 500 μ, even the model of tower was reused repeatedly.

4.3. Evaluation of fatigue life

The equivalent numbers of cycle were calculated based on Miner's rule [20] shown in Eq. (4) for G-S-900 and G-D-900 because amplitude of input acceleration was increased step by step for these cases.

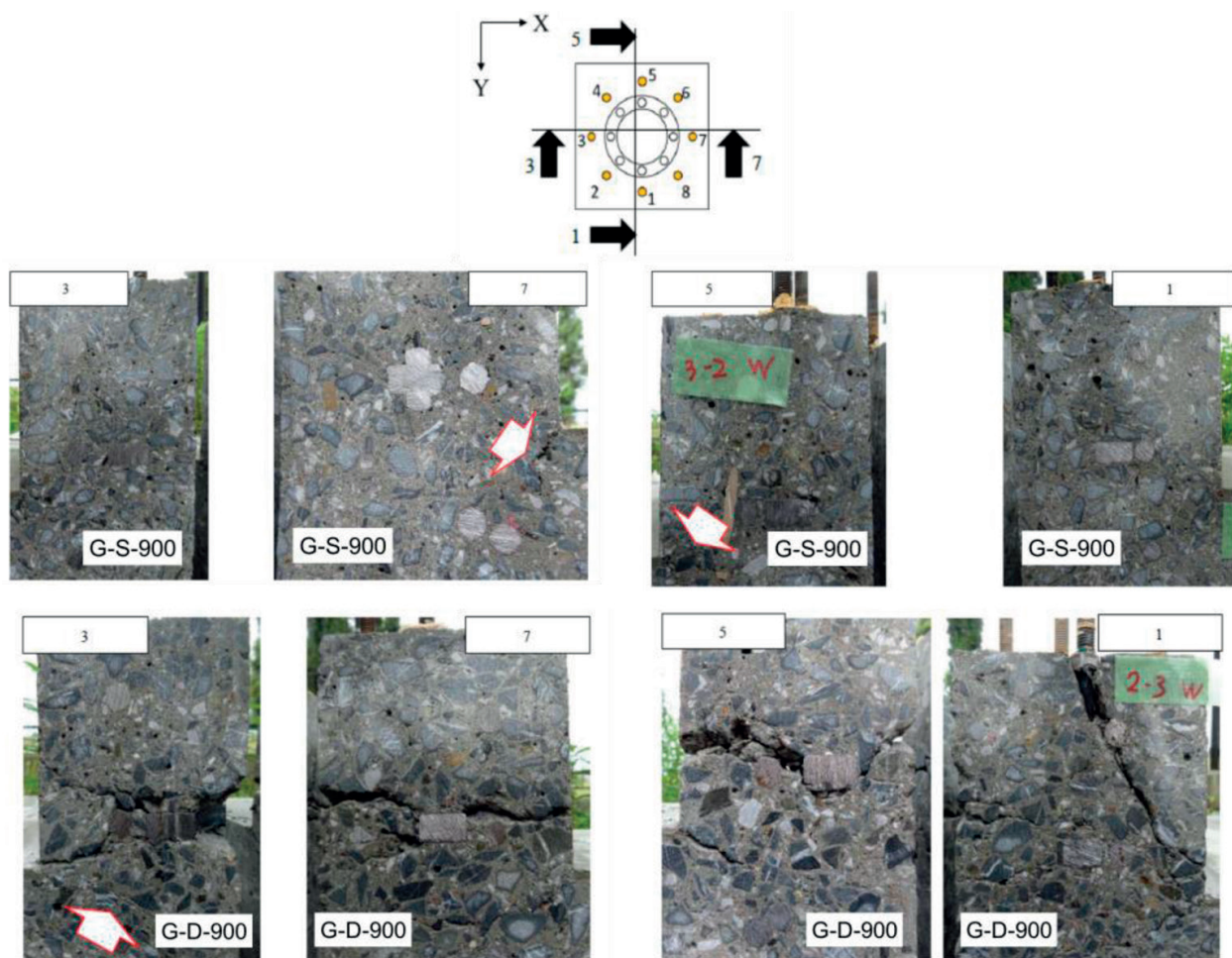$$N_{eq} = \sum_{i=1}^{n} \left(\frac{P_i}{P} \right)^m \cdot n_i \tag{4}$$

Figure 17. Internal cracks observed after loading for G-S-900 and G-D-900.
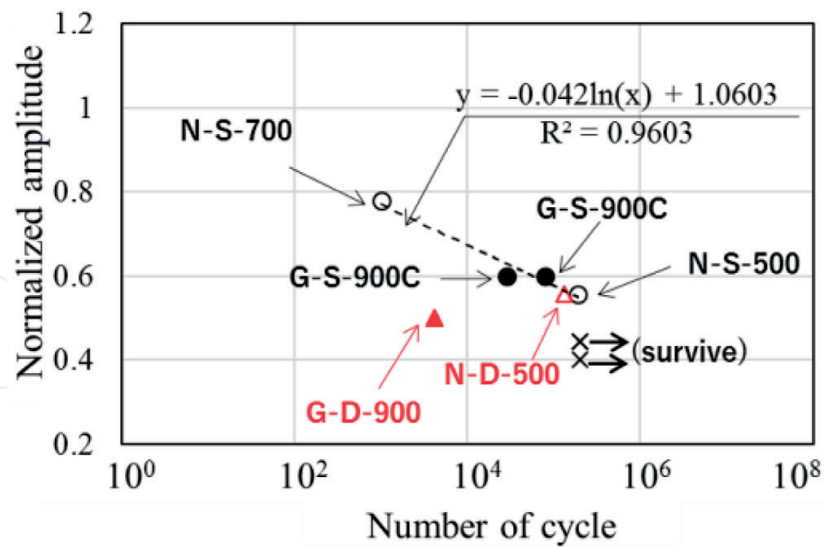
Figure 18. Normalized amplitude of horizontal load—cycles at failure based on experiment.

where N_{eq} is the equivalent number of cycle, P_i is the load, P is the standard load, n_i is the number at P_i, m is the incline of material stress-number of cycle (S-N) curve for fatigue. The m was assumed as 17 based on the S-N curve for fatigue of concrete [20]. If we assume P = 900 gal, the N_{eq} is 28,378 for G-S-900 and the N_{eq} is 4098 for G-D-900.

Furthermore, the difference of experiment conditions between "N-" series and "G-" series should be considered for evaluation. The ultimate load that can make collapse of structure at one cycle should be different in two series. The ultimate acceleration that is proportional to ultimate inertial force at the top of tower was assumed as 800 gal and 1300 gal for "N-"and "G-," respectively.

The number of cycles at each normalized amplitudes in this experiment was summarized in **Figure 18**. The approximate curve for single directional vibration is also shown in the figure. According to this figure, the fatigue life of the specimens vibrated in two directions; N-D-500 and G-D-900 tend to be shorter than lives under single directional vibration.

5. Conclusions

This chapter shows research of stability of supporting structure of onshore wind turbine foundations based on field measurements, finite element (FE) analysis and laboratory experiment. The vibration characteristics of tower were clarified by field measurement. Then, the damage process of reaching failure was examined by FE models. In addition, limit state of foundation was defined by fatigue limit state of concrete. The space-averaged second invariant of strain was proposed as useful index. Consequently, the stress-number of cycle (S-N) diagram derived from laboratory experiment was shown. That suggested that the fatigue life of the specimens vibrated in two directions tends to be shorter than lives under single directional vibration.

Acknowledgements

Author details

Chikako Fujiyama[1]*, Yasuhiro Koda[2] and Noriaki Sento[2]

*Address all correspondence to: fujiyama@hosei.ac.jp

1 Department of Civil and Environmental Engineering, Faculty of Design and Engineering, Hosei University, Tokyo, Japan

2 Nihon University, Koriyama, Fukushima, Japan

References

[1] Global Wind Energy Council. Global Wind 2007 Report, GWEC 2008

[2] Global Wind Energy Council. Global Wind 2016 Report, GWEC 2017

[3] http://www.caithnesswindfarms.co.uk/AccidentStatistics.htm [Accessed: February 09, 2018]

[4] Alonso TR, Dueñas EG. Crack analysis in onshore wind turbine foundations. IABSE Madrid Symposium Report. 2014;**102**:1086-1092

[5] Currie M, Saafi M, Tachtatzis C, Quail F. Structural integrity monitoring of onshore wind turbine concrete foundations. Journal of Renewable Engergy. 2015;**83**:1131-1138

[6] Hassanzadeh M. Cracks in onshore wind power foundations – causes and consequences. Elforsk Rapport. 2012;**11**:56

[7] Chijiwa N, Hong TM, Iwanami M, Saito T, Yamaya A, Motegi H, Shinozaki H. Rapid degradation of concrete anchorage performance by liquid water. Journal of Advanced Concrete Technology. 2015;**13**(10):438-448

[8] Bai X, He M, Ma R, Huang D, Chen J. Modelling fatigue degradation of the compressive zone of concrete in onshore wind turbine foundations. Journal of Construction and Building Materials. 2017;**132**:425-437

[9] Unobe ID, Sorensen AD. Multi-harzard analysis of a wind turbine concrete foundation under wind fatigue and seismic loadings. Jounal of Structural Safely. 2015;**57**:26-34

[10] Yonetsu K, Fujiyama C, Kado M, Maeshima T, Koda Y. Fatigue evaluation for RC foundation of wind turbine based on field measurement and nonlinear FE analysis. Journal of JSCE E2. 2016;**72**(2):68-82 (in Japanese)

[11] Swarzt RA, Lynch JP, Zerbst S, Sweerman B, Rolfes R. Structural monitoring of wind turbines using wireless sensor networks. Smart Structural and System. 2010;**6**(3):183-196 (USA)

[12] Rumsey MA, Paquette JA. Structural Health Monitoring of Wind Turbine Blades. Albuquerque: Sandia National Laboratories; 2007

[13] Fujiyama C, Yonetsu K, Maeshima T, Koda Y. Identifiable stress state of wind turbine tower-foundation system based on field measurement and FE analysis. Procedia Engineering. 2014;**95**:279-289

[14] Maekawa K, Toongoenthong K, Gebreyouhannes E, Kishi T. Direct path integral scheme for fatigue simulation of reinforced concrete in shear. Journal of Advanced Concrete Technology. 2006;**4**(1):159-177

[15] Maekawa K, Gebreyouhannes E, Mishima T, An X. Three-dimensional fatigue simulation of RC slabs under traveling wheel-type loads. Journal of Advanced Concrete Technology. 2006;**4**(3):445-457

[16] Shimodate H, Fujiyama C, Koda Y, Kado M. Analysis of vibration characteristic of wind turbine and prediction of failure mode of footing-tower direct connection system. In: Proceedings of 71st Annual Conference of JSCE; 2016. pp. 13-14 (in Japanese)

[17] Saitoh S, Maki T, Tsuchiya S, Watanabe T. Damage assessment of RC beams by nonlinear FE analyses. Journal of JSCE E2. 2011;**67**(2):166-180 (in Japanese)

[18] Yonetsu K, Fujiyama C, Koda Y, Maeshima T. Strain index for wind turbine tower-foundation joint by using nonlinear FE analysis. In: Proceedings of 70th Annual Conference of JSCE; 2015 (in Japanese)

[19] Ueda Y, Fujiyama C, Sentoh N, Koda Y. Fatigue experiment of wind turbine tower-foundation joint by using shaking table. In: Proceedings of 71st Annual Conference of JSCE; 2016. No. CS3-008 (in Japanese)

[20] Japan Society of Civil Engineers. Standard Specification for Concrete Structures 2007. Design; 2007